Available online at www.sciencedirect.com
SCIENCE DIRECT®
C. R. Chimie 8 (2005) 147–156
COMPTES RENDUS CHIMIE
http://france.elsevier.com/direct/CRAS2C/

Full paper / Mémoire

Phase diagrams and structures of HgX_2 (X = I, Br, Cl, F)

Marc Hostettler [a], Dieter Schwarzenbach [b,*]

[a] *Laboratorium für chemische und mineralogische Kristallographie, University of Bern, Freiestrasse 3, CH-3012 Bern, Switzerland*
[b] *Laboratoire de cristallographie, École Polytechnique Fédérale de Lausanne, CH-1015 Lausanne, Switzerland*

Received 7 January 2004; accepted after revision 23 June 2004

Available online 07 January 2005

Abstract

The structures and the phase diagrams as functions of temperature and pressure of the solid mercury(II) halides known to date are reviewed. HgI_2 adopts an amazing number of stable and metastable tetrahedral-framework semiconductor and molecular structures. It also possesses the most complicated phase diagram. It realizes four of the six simplest structures where the iodine atoms form a cubic close-packing and the mercury atoms are located in corner-sharing tetrahedral voids, with close to tetrahedral I–Hg–I and Hg–I–Hg bond angles. Hg atoms appear to be able to diffuse between tetrahedra. There also exists a metastable structure composed of straight HgI_2 molecules, which is kinetically favoured during crystallization from solution. The high-temperature and the high-pressure structures show bent molecules. $HgBr_2$ forms molecular structures with packings similar to the HgI_2 molecular structures, except phase IV at pressures above 3.9 GPa, which is a modulated CdI_2-type layer structure with trigonal-pyramidal and octahedral coordinations of Hg. The three known molecular structures of $HgCl_2$ show straight or bent molecules whose packings differ from those of the bromide and iodide. HgF_2 adopts a fluorite-type structure. Whereas the analogous Zn and Cd compounds roughly obey the classical ionic radii-ratio rules, there are several preferred coordination types in the Hg(II) halides. ***To cite this article: M. Hostettler, D. Schwarzenbach, C. R. Chimie 8 (2004)***.

Résumé

Diagrammes de phase et structures des composés HgX_2 (X = I, Br, Cl, F). Ce travail présente les structures cristallographiques des dihalogénures de mercure solides, HgX_2, connues à ce jour ainsi que leurs diagrammes de phase en fonction de la température et de la pression. On distingue deux classes de structure radicalement différentes : (*i*) les structures réticulaires semi-conductrices et (*ii*) les structures moléculaires formées par des empilements de molécules HgX_2 linéaires ou angulaires. Dans la classe (*i*), les ions halogénure X forment des empilements compacts de sphères presque parfaits. HgI_2 présente le diagramme de phase le plus compliqué. Dans les conditions ambiantes, ce composé cristallise à partir de solvants organiques ou par sublimation, successivement en trois modifications : jaune (classe *ii*) puis orange (classe *i*) métastables, et finalement rouge (classe *i*), thermodynamiquement stable. La forme rouge se construit par des couches de tétraèdres $[HgI_4]$ liés par leurs sommets. La forme orange englobe trois structures différentes dont les unités sont des supertétraèdres $[Hg_4I_{10}]$ liés par leurs sommets. Deux de ces structures sont des complications fractales de la structure rouge. Les quatre structures tétraédriques ont en

* Corresponding author.
E-mail addresses: marc.hostettler@krist.unibe.ch (M. Hostettler), dieter.schwarzenbach@epfl.ch (D. Schwarzenbach).

1631-0748/$ - see front matter © 2004 Académie des sciences. Published by Elsevier SAS. All rights reserved.
doi:10.1016/j.crci.2004.06.006

commun la symétrie tétragonale, l'empilement compact cubique des I, et la première sphère de coordination de tous les atomes. Tous les angles Hg–I–Hg et I–Hg–I sont tétraédriques (~ 109°) et les distances interatomiques sont très semblables. Deux autres structures simples possèdent les mêmes propriétés ; l'une est connue pour $ZnCl_2$ mais pas pour HgI_2, tandis que l'autre n'a pas été observée. Les atomes de Hg sont mobiles et peuvent diffuser entre les lacunes tétraédriques. Aux températures et pressions élevées, HgI_2 présente des molécules angulaires, tandis que les molécules de la modification jaune métastable sont linéaires. Il existe aussi une transition anti-isostructurale entre deux phases de structure rouge, caractérisée par une changement discontinu de la « tétragonalité » *c/a*. $HgBr_2$ ne change pas de structure en fonction de la température, mais possède plusieurs phases sous différentes pressions, dont deux des structures sont connues : l'une est moléculaire et identique à celle de la phase jaune métastable de HgI_2, la seconde est une structure octaédrique du type CdI_2, modifiée par une modulation commensurable qui amène à des coordinations octaédriques et trigonales–pyramidales. En fonction de la pression, $HgCl_2$ présente plusieurs structures moléculaires linéaires ou angulaires, dont les empilements diffèrent de ceux observés pour les phases moléculaires de HgI_2 ou $HgBr_2$. HgF_2, enfin, présente une structure de type CaF_2 (fluorite). Une comparaison avec les dihalogénures de Zn et de Cd montre que les structures de HgX_2 sont loin d'être ioniques (à l'exception de HgF_2), tandis que les composés analogues de Zn et de Cd adoptent des coordinations obéissant, au moins partiellement, aux règles classiques des composés ioniques. ***Pour citer cet article : M. Hostettler, D. Schwarzenbach, C. R. Chimie 8 (2004)***.

Keywords: Mercury halides; Phase diagram; Phase transition; High pressure; Polymorphism

Mots clés : Halogénures de mercure ; Diagramme de phase ; Transition de phase ; Haute pression ; Polymorphisme

1. Introduction

The mercury(II) halides, HgX_2 with X = I, Br, Cl and F, form an amazing number of solid phases and adopt remarkably different crystal structures. In this contribution, we review the structures of these compounds known to date and their geometric relations. We also present the corresponding pressure–temperature phase diagrams. The structures of solid HgX_2 fall into two very different classes: (*i*) semiconductor-type framework structures where the anions X form nearly ideal closest sphere packings, and (*ii*) structures built from linear or bent HgX_2 molecules where the anions X form very distorted close packings.

HgI_2 exhibits the largest diversity of structures. This compound has been extensively studied by many techniques in view of its opto-electronic properties and the technological interest has resulted in several hundreds of publications that have been reviewed in [1]. At ambient conditions, HgI_2 adopts structures of both classes. The stable red phase forms a tetrahedral close-packing structure. It is used as room-temperature detector material for X- or γ-rays [2–4]. Besides, there exist two metastable forms at ambient conditions, an orange one of class (*i*) and a yellow one of class (*ii*). The known high-temperature and high-pressure phases are molecular. $HgBr_2$ is also a candidate material for the detection of photons [5], but has been much less investigated in comparison to HgI_2. At ambient pressure, this compound adopts a molecular class-(*ii*) structure, whereas at high pressure it forms a modulated CdI_2-type class-(*i*) structure with octahedral and pyramidal coordinations of Hg. Several high-pressure phases with unknown structures also exist. For $HgCl_2$, only molecular class-(*ii*) structures are known. Pure water-free HgF_2 is difficult to prepare, and therefore its phase diagram is not known. At ambient conditions, it forms a fluorite-type (CaF_2) structure built from corner-linked HgF_8 cubes.

2. Mercuric iodide

2.1. Polymorphism of HgI_2 at ambient conditions

Mercuric iodide (HgI_2) is known to crystallize from various organic solvents and also by sublimation into three concomitant polymorphs whose colours are red, orange, and yellow [6]. At ambient conditions, the red phase is thermodynamically stable, while the orange and yellow phases are metastable and transform into the red phase when touched. The aspects and speeds of these transformations are different for the two forms. In the orange crystals, red nuclei develop into domains of irregular shape, which spread and transform a crys-

tal of diameter 0.2 to 0.5 mm within hours or days while preserving the external shape. In contrast, in the yellow form, a sharp red front propagates from the contact point and consumes all of a crystal of dimensions 0.2 to 0.5 mm within a few seconds while the crystal may warp. From a 2-chloroehtanol solution, the yellow crystals are the first, and the red crystals the last to crystallize, as observed by optical microscopy [7]. Faster evaporation favours the formation of yellow crystals. Above 323 K, only yellow crystals are formed, whereas slow crystallization in a closed vessel gives only red, orange or red-orange composite crystals.

2.2. Crystal structures of the polymorphs at ambient conditions

The structures of the polymorphs of HgI_2 at ambient conditions are shown in Fig. 1; Table 1 lists unit cell parameters and space group symmetries. All the structures of the red and the orange phases have in common a nearly ideal cubic closest packed (*ccp*) substructure of iodine atoms with 1/4 of the tetrahedral interstices occupied by Hg. The HgI_4 tetrahedra are corner-linked and all Hg–I–Hg and I–Hg–I angles are close to tetrahedral. There is only one kind of Hg atom, i.e. all tetrahedra (but not all corners, i.e. iodine atoms) are symmetry-equivalent. It can be shown that six different structures with these properties, all of them tetragonal, can be derived from a *ccp*-array of anions (at least two such structures exist for the hexagonal *hcp* array with space group symmetries $Pmc2_1$ and *Pbam*; to our knowledge, they have never been observed experimentally). Four of these six structures are realized by HgI_2; one of remaining structures has not (yet) been identified for HgI_2 but is realized by $ZnCl_2$; a sixth structure has never been observed. The stable red form consists of layers of corner-linked HgI_4 tetrahedra [8,9], stacked by I···I contacts. The metastable orange crystals com-

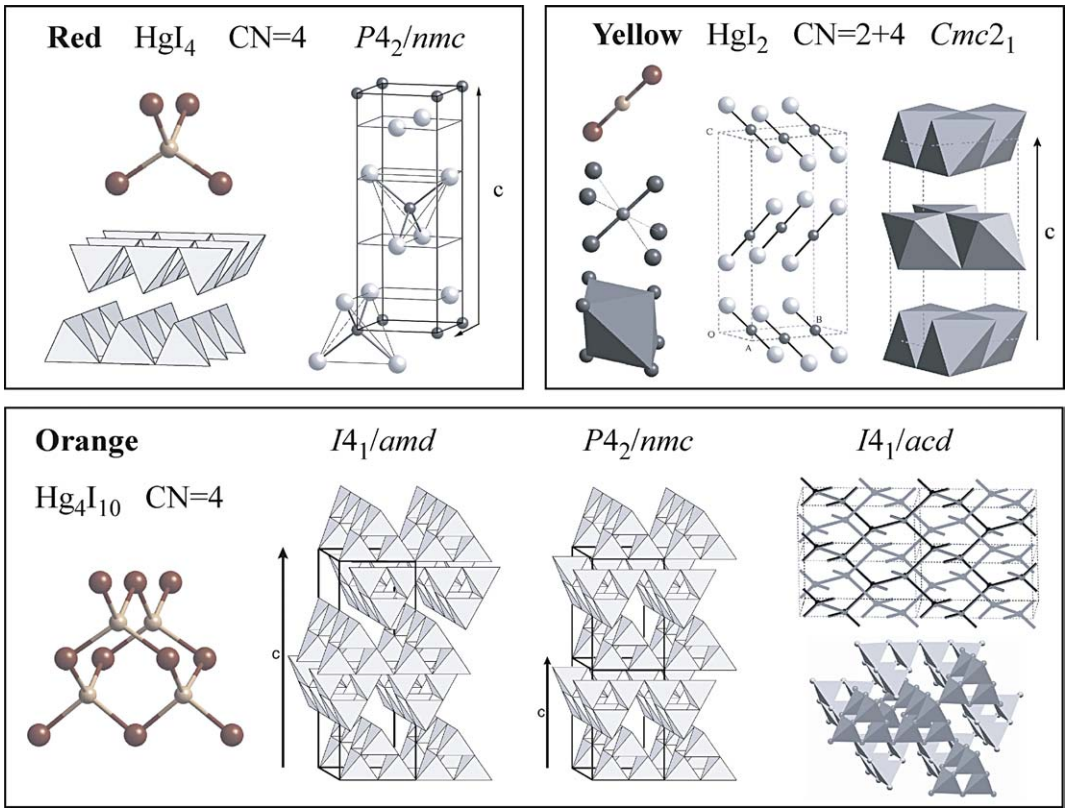

Fig. 1. Structures of the polymorphs of HgI_2 at ambient conditions. The red phase (III of Fig. 2) is thermodynamically stable. The orange phase comprises three different structures built of corner-shared Hg_4I_{10} supertetrahedra. The two layered structures are end-members of a polytypic family with layer symmetry $P\bar{4}m2$. In the third structure, the supertetrahedra form two interpenetrating three-dimensional networks.

Table 1
Space-group symmetries and unit-cell dimensions of the solid phases of the halides HgX_2. The subscript M indicates a metastable phase obtained at ambient conditions, ac stands for ambient conditions, HT for high temperature, HP for high pressure

	Phase	Space group	*a* (Å)	*b* (Å)	*c* (Å)	*β* (°)	Reference
HgI_2	III at *ac*, red	$P4_2/nmc$	4.361(5)	–	12.450(7)	–	[9]
HgI_2	$orange_M$ MDO1	$I4_1/amd$	8.7860(9)	–	24.705(9)	–	[10]
HgI_2	$orange_M$ MDO2	$P4_2/nmc$	8.7860(9)	–	12.353(5)	–	[10]
HgI_2	$orange_M$ D	$I4_1/acd$	12.3930(18)	–	24.889(5)	–	[11]
HgI_2	$yellow_M$	$Cmc2_1$	4.734(1)	7.408(2)	13.943(3)	–	[7]
HgI_2	II, $yellow_{HT}$, 141(1) K	$P2_1$	8.0206(7)	13.9239(7)	4.4081(3)	95.062(6)	[7]
HgI_2	IV, red, 0.8(1) GPa	$P4_2/nmc$	4.334(3)	–	12.178(2)	–	[18]
HgI_2	VI, $yell_{HP}$, 1.8(1) GPa	$P2_1/a$	13.948(3)	5.343(2)	5.113(2)	106.51(2)	[18]
HgI_2	VII, 11.0(1) GPa	*hexag/trig*	8.441(2)	–	12.073(3)	–	[18]
$HgBr_2$	I at *ac*	$Cmc2_1$	4.628(2)	6.802(2)	12.476(2)	–	[24]
$HgBr_2$	IV, 5,4(1) GPa	$P3$	6.7569(3)	–	5.6589(9)	–	[27]
$HgBr_2$	V, 10.7(1) GPa	hexag/trig	6.787(1)	–	11.130(2)	–	[27]
$HgCl_2$	I, *ac*	*Pnma*	12.776(4)	5.986(3)	4.333(2)	–	[28]
$HgCl_2$	V, 572(1) K	*cubic*	4.41(2)	–	–	–	[29]
$HgCl_2$	IV, 1.7(1) GPa	$P2_1/m$	12.378(2)	5.711(1)	8.369(1)	91.01(5)	[29]
$HgCl_2$	II, 2.2(1)GPa	$R\bar{3}m$	5.569(1)	–	7.817(1)	–	[29]
HgF_2	I, *ac*	$Fm\bar{3}m$	5.54(1)	–	–	–	[32]

prise three different crystal structures, all of which are built from corner-linked Hg_4I_{10} supertetrahedra [10,11]. Two of them are end members with the maximum degree of order (MDO) of a polytypic layer structure; the third shows a three-dimensional diamantoid-type linkage (D). The two MDO structures are fractal complications of the stable red form of HgI_2 obtained by replacing single tetrahedra by supertetrahedra. The geometries and anisotropic displacement parameters of the layers in MDO1 and MDO2 and the interlayer contacts are nearly identical in the two stackings [10]. The two MDO structures usually coexist and form a disordered crystal. A quantitative analysis of the stacking disorder by fitting a Markov chain model to the intensities of the corresponding rods of diffuse X-ray scattering suggests the presence of nearly equal volumes of the MDO structures with an average domain thickness of about five layers or 30 Å [10]. The third orange structure D (diamantoid) is also composed of corner-linked Hg_4I_{10} supertetrahedra. However, the supertetrahedra are not linked into layers but into two interpenetrating four-connected three-dimensional networks [11]. This is the fractal complication of the structure of $ZnCl_2$. Composite crystals containing all three supertetrahedral structures MDO1, MDO2 and D, twinned in three perpendicular directions resulting in a pseudocubic edifice, have also been observed [11].

In contrast to the red and orange forms, the structure of the yellow metastable ($yellow_M$) polymorph at room temperature is molecular with linear I–Hg–I molecules (angle 180.4° not constrained by symmetry) [7,9]. Not surprisingly, the packing of the iodine atoms is very distorted. Closest-packed layers with six-coordinated spheres are stacked roughly midway between *ccp* and *hcp*. Therefore, the iodine substructure may be described as related to the cubic volume-centred *bcc* structure [7]. The coordination of mercury by iodine is very distorted octahedral 2+4, with two close and four considerably more distant neighbours.

2.3. Mechanisms of crystallization and transformation of HgI_2

When crystallizing HgI_2 at ambient conditions, rapid evaporation of the solvent is essential for the formation of the $yellow_M$ polymorph, indicating that the crystallization of this form is governed by kinetics. Raman spectra of an HgI_2 solution in 2-chloroethanol indicate HgI_2 to exist in the form of molecules [7]. Therefore, the observed crystallization sequence can be understood as a kinetic effect: the pre-existing molecules rapidly pack into the $yellow_M$ form, while the formation of HgI_4 tetrahedra demands the breaking of bonds. On the other hand, it remains unclear why the orange structures are kinetically favoured and formed before the stable red structure. In both structures, there are four shortest Hg–Hg distances, but the Hg distribution in

the orange forms is globular and somewhat more homogeneous than the planar distribution in the red form. It seems reasonable that the formation of clusters with limited dimensions is kinetically favoured over the formation of extended sheets. The choice between the different non-layer structures does not seem to be dominated by electrostatic interactions; we would expect the $ZnCl_2$ structure, which is not realized by HgI_2, to have the largest Madelung energy of the six tetrahedral structures mentioned above and thus to be the most ionic one. We also note that ZnI_2 at ambient conditions forms the supertetrahedral D-structure. The transformations from orange to red presumably involve only movements of Hg atoms in an invariant *ccp* matrix of I. The thermal displacement parameters of Hg in the tetrahedral structures are indeed larger than those of iodine [10,11]. In contrast, the transformation from $yellow_M$ to red implies a complete rearrangement of the atoms.

2.4. Phase diagram of HgI_2

The phase diagram of HgI_2 has been investigated by many authors with different techniques. The somewhat controversial results are reviewed in [12]. A phase diagram compiled from all the various experimental observations is presented in Fig. 2. Five different phases (I, II, III, IV, VI) are reported in the moderate pressure–temperature range of $p < 4$ GPa, $T < 700$ K, the boundaries of which have been established by dilatometry (compression-curve method) [13], differential thermal analysis [14], Raman spectroscopy [15,16] and powder X-ray diffraction [17,18].

At 400 K and ambient pressure, the red form discussed above (phase III) undergoes a reconstructive transition to the yellow high-temperature phase II ($yellow_{HT}$), which has been assumed to be identical to the $yellow_M$ polymorph obtained under ambient conditions [12]. However, we have observed the symmetry of the $yellow_{HT}$ phase to be $P2_1$, a subgroup of the space group $Cmc2_1$ of the $yellow_M$ structure. The two structures are closely related; both show similarly packed I–Hg–I molecules. The main difference consists in the molecules in $yellow_{HT}$ being bent and not linear (Fig. 3), with angles of 163(1)° and 157(1)° for the two molecules in the asymmetric unit. Electron diffraction and vibrational spectroscopy cannot rule out the existence of slightly bent molecules in the gas phase (165–180°); ab initio studies usually assume straight molecules [19]. The mechanisms of the III → II and the reverse II → III transitions are different. Upon heating, the transition occurs through surface nucleation while, upon cooling, it shows bulk nucleation [20]. The kinetics of the II–III transition is highly asymmetric. The growth rate of a newly formed crystal has been measured by the increase of a normalized integrated Bragg intensity with time, $(\Delta I_{Bragg}/I_{Bragg})$ (s^{-1}). For III→II, the growth rates of phase II at 402.9 and 404.0 K are 3.6×10^{-4} s^{-1} and 4.2×10^{-4} s^{-1}, respectively. In contrast, for II→III, the growth rate at 381.0 K is much smaller, 1.8×10^{-5} s^{-1} [7]. The hysteresis of the transition is also asymmetric in the sense that phase II can be undercooled to room temperature, while the red phase can be overheated by only about 10 K above the transition temperature [7]. The II–III phase boundary presents the particularity of a maximum at about 0.5 GPa (Fig. 2). The volumetric data of Bridgman [13] show that there is no change of volume when crossing the transition line at the maximum of 0.5 GPa. At lower pressures, phase II is less

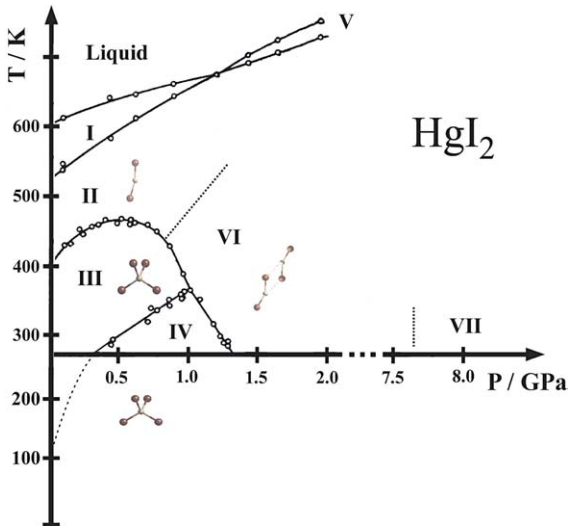

Fig. 2. Phase diagram of HgI_2. The phase boundaries have been established by differential thermal analysis (circles) [14]. The dotted line delimiting phases II and VI has been found by Raman spectroscopy [16]. The VI–VII transformation has been identified by X-ray diffraction, its boundary has been mapped only at room temperature [17]. The III–IV boundary is extrapolated from DTA data [14] to the transition point observed by X-ray diffraction at ambient pressure [18]. The corresponding structural motifs, if known, are shown in the stability regions of the phases. Powder X-ray diffraction data of phase VII indicate a hexagonal cell. No diffraction data exist for phases I and V and the existence of phase I has not been clearly established [12].

dense than phase III, while at higher pressures phase II is denser. In addition, phase II presents a higher compressibility than phase III over the whole pressure range up to 1 GPa. This peculiar combination of higher compressibility of the denser phase is also observed for ice and water.

Several of the high-pressure structures have been determined, at least qualitatively [17,18,21]. Differential thermal analysis data [14] show the existence of a transition between the red phase III and another red phase IV at moderate temperatures and pressures (Fig. 2). Powder diffraction data collected as a function of pressure at room temperature show that the III–IV transformation is neither associated with a change of space group symmetry nor with a discontinuous change of volume of the unit cell. Instead, it shows two different 'tetragonalities' [18]: the slope of the change of the *c*/*a* ratio with pressure, and also with temperature, is discontinuous at the phase boundary, while $c/a - 2\sqrt{2}$ changes sign. All observations obtained with various experimental techniques [18] may be explained by assuming that the III–IV transformation is an anti-isostructural transition [22].

Upon further increasing the pressure at room temperature, the red phase (III, IV) undergoes a transition to a yellow$_{HP}$ phase VI at about 1.2 GPa. At room temperature, phase VI is stable up to 7.7 GPa, at which pressure a transformation to phase VII occurs. Based on the first published diffraction data at high pressure [17], obtained with a sealed Mo tube and X-ray film, phase VI was proposed to be identical with phase II, and phase VII a polytypic variant of the CdI_2 structure. Later Raman spectroscopy data disproved the identity of phases II and VI and the corresponding phase boundary was established [16]. The most recent diffraction experiments carried out with synchrotron radiation and area detector showed that the structure of phase VI is another variant of the yellow molecular phase [18,21], showing bent HgI_2 molecules that form dimers (Fig. 3). Powder diagrams of phase VII at 11.0 GPa could be indexed with a hexagonal cell, *c*/*a* = 1.43 [18]. The data did not allow to solve the structure; for a CdI_2-type structure *c*/*a* ~ 1.6.

3. Mercuric bromide

3.1. Phase diagram of $HgBr_2$

At ambient conditions, the stable phase I of $HgBr_2$ adopts the same structure as the yellow metastable polymorph of HgI_2 [23,24]. At ambient pressure, no phase transitions have been reported, phase I being stable from 90 K, the lowest temperature investigated, to the melting temperature of 509 K. The application of pressure up to 4.5 GPa induces several transitions as revealed by dilatometry (compression-curve method) [25] and Raman spectroscopy [26]. Three phases (II, III, IV) have been reported in this pressure range (Fig. 4). The crystal structure of phase IV has recently been solved making use of synchrotron data, and an additional phase V above 9 GPa was identified [27].

3.2. Phase transition sequence under pressure

The I–II transition was first detected by dilatometry. It is accompanied by a volume change similar to the one observed for the II–III and III–IV transitions [25].

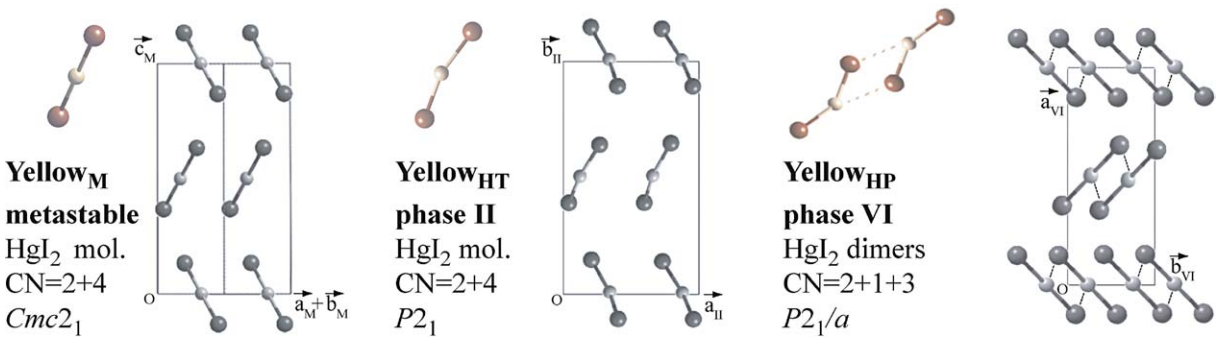

Fig. 3. Structures of the yellow molecular phases of HgI_2.

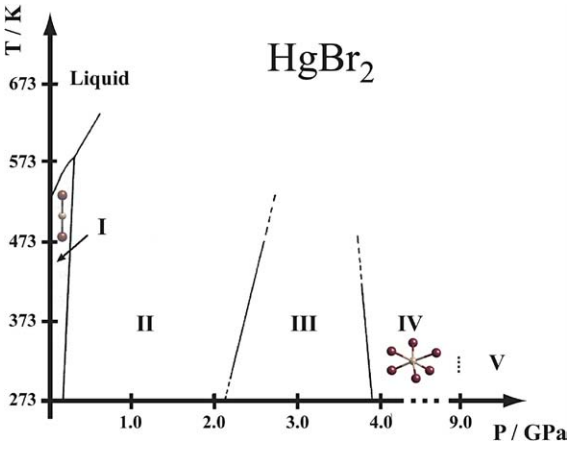

Fig. 4. Phase diagram of $HgBr_2$. The phase boundaries between phases I to IV have been established by Raman spectroscopy [26]. The IV–V phase transition has been identified by X-ray diffraction [27].

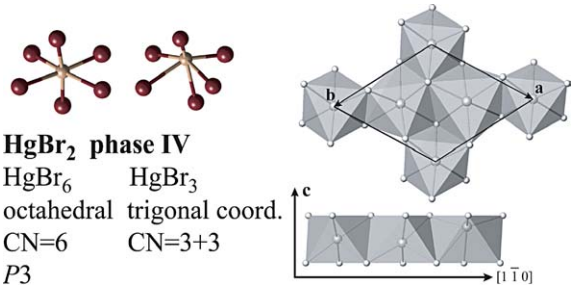

Fig. 5. Structure of the trigonal phase IV of $HgBr_2$ at 5.4 GPa showing layers of edge-shared octahedra. Note the alternation of the three mercury sites along the [1 $\bar{1}$ 0] direction.

However, its existence was not conclusively confirmed by Raman spectroscopy [26] or by X-ray diffraction [27]. Phase III displays a more complicated diffraction pattern than phase I, additional powder lines suggesting a lower, possibly monoclinic symmetry. Attempts to index the pattern were unsuccessful. In addition, the corresponding Raman spectrum shows an inferior signal-to-noise ratio compared to the spectra from I, II and IV [26]. These difficulties might indicate the formation of a strongly disordered state within the stability range of phase III. The III–IV transition has a destructive character and leads to a well-defined powder pattern of a trigonal phase IV, the structure of which is a variant of the CdI_2-type. It is built from layers of edge-sharing octahedra that are stacked by Br···Br contacts. In contrast to the CdI_2-type structure, some of the coordinated metal atoms are displaced along *c* from the centroids of the octahedra, leading to three distinct mercury sites (Fig. 5). One of the three Hg atoms adopts a trigonal-pyramidal coordination with three nearest neighbours, whereas the other two show an approximately octahedral coordination with six bonds of roughly the same length [27]. The structure of phase IV may be described as a commensurate modulation of the CdI_2 structure.

4. Mercuric chloride

4.1. Structure of $HgCl_2$ at ambient conditions

At ambient conditions, the structure of $HgCl_2$ (phase I) is molecular with straight Cl–Hg–Cl molecules [28] that form herringbone layers in the mirror plane of the space group *Pnma* (Fig. 7). This structure is not related to HgI_2-yellow$_{HT}$ and ambient $HgBr_2$. The coordination of Hg is 2 + 6 (rather than 2 + 4) forming a distorted rhombohedron. The smallest distance between chlorine atoms of adjacent molecules is less than the sum of the van der Waals radii of Cl suggesting attractive Cl···Cl interactions. The lattice parameters of phase I may be expressed as an orthorhombic distortion of a cubic closest packing of chlorine atoms (Table 1).

4.2. Phase diagram

Upon increasing temperatures at ambient pressure, the lattice constants show a decrease of the orthorhombic distortions of phase I, followed by a transition to a cubic phase V at 572 K, three degrees below the melting temperature [29]. The structure of phase V has not been investigated in detail; one might consider Hg to be disordered over, or diffusing between, voids of the cubic closest packing of Cl atoms.

Infrared, Raman [30] and NQR [31] spectroscopy revealed the existence of two high-pressure phases between 0 and 2.5 GPa at room temperature (Fig. 6). The structures of these two high-pressure phases have recently been determined from X-ray powder diffraction with synchrotron radiation [29]. At ambient temperature, $HgCl_2$ undergoes a continuous transition to a monoclinic phase IV at 0.7 GPa. The structure of this phase is a slight monoclinic distortion of the orthorhombic phase I, $\beta = 91.01(5)°$ at 1.7 GPa, whereby the

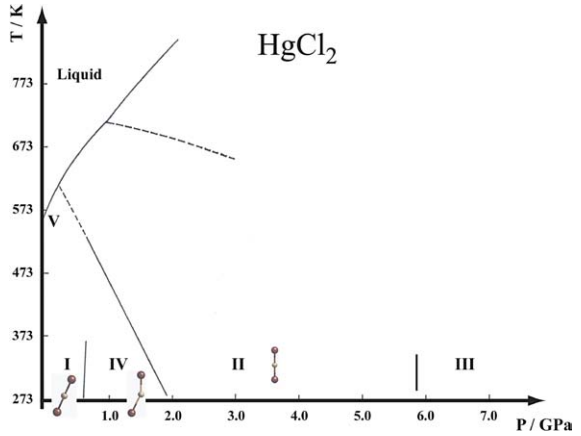

Fig. 6. Phase diagram of $HgCl_2$. The phase boundaries have been established by Raman spectroscopy, adapted from [30]. The nomenclature of the phases adopted in [30] has been retained.

mirror plane is preserved. There are four symmetry independent Cl–Hg–Cl molecules placed on the mirror that are now bent (Fig. 7). Phase IV is stable up to 2.1 GPa, at which pressure a first-order transition occurs to a rhombohedral $R\bar{3}m$ phase II showing straight molecules. Phase II is stable up to 6.0 GPa, at which pressure new powder lines appear in addition to those of the $R\bar{3}m$ phase. These lines have been attributed to phase III. Surprisingly, phases II and III coexist at least up to 20 GPa.

5. Mercuric fluoride, structure of HgF_2 at ambient conditions

At ambient conditions, HgF_2 adopts the cubic CaF_2-type structure [32] consisting of corner-sharing HgF_8 cubes (Table 1, Fig. 8). So far, no information has been published on the phase diagram. Our attempt [29] to investigate the behaviour of this compound under pressure failed due to the fact that all available samples were hydrated.

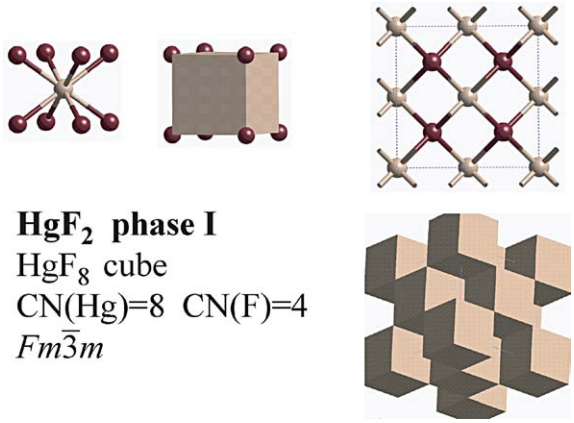

Fig. 8. Structure of the fluorite-type phase of HgF_2 at ambient conditions [32].

6. Discussion

The results presented here show that mercury(II) does not have a single preferred coordination with non-metallic elements. The numerous known structures of its four halides HgX_2 show coordination numbers (CN) between two and eight. Coordinations of Hg include CN = 2 + 4 or 2 + 6 for linear or bent X–Hg–X molecules, tetrahedral CN = 4, trigonal pyramidal CN = 3 + 3 and octahedral CN = 6, and cubic CN = 8. HgI_2 adopts many of these structures. At low pressures and temperatures, the coordination is tetrahedral, with CN = 4 and nearly perfect *ccp* packing of the iodine atoms. In this packing, Hg appears to be able to move between tetrahedral voids. High temperature and pres-

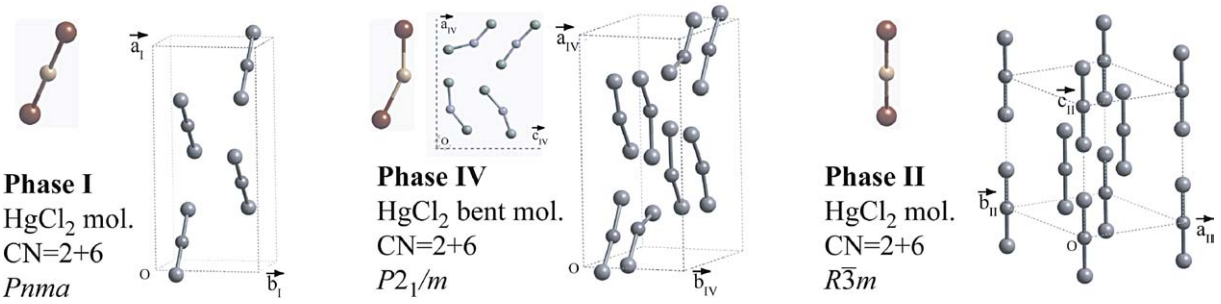

Fig. 7. Structures of the molecular phases of $HgCl_2$, phase I at ambient conditions, phases IV and II at high pressure. In phase IV, the molecules occupy the *a/c* mirror plane.

sure stabilizes molecular structures with CN = 2 + 4 and bent I–Hg–I molecules. Above 7.7 GPa, the metric is hexagonal, but the lattice constants do not seem to correspond to a framework structure related to e.g. the CdI_2 type. $HgBr_2$ does not form tetrahedral structures. It favours molecular structures with CN = 2 + 4 in the low-pressure region, while pressures above 4.0 GPa stabilize pyramidal and octahedral coordinations. Two uncharacterized phases occur at intermediate pressures. $HgCl_2$ forms only straight or bent molecular structures, but with a distorted rhombohedral coordination CN = 2 + 6. No information is available on the phase diagram of HgF_2; the cubic phase I might be stable at high pressure. This is the only structure that could be interpreted as ionic.

It is interesting to compare these results with the halides of the other group IIB elements Zn and Cd [33]. These compounds do not form molecular structures. ZnF_2 adopts the rutile structure, and the other halides form tetrahedral structures with closest-packed anions [33–37]. We recall that there are six simple tetrahedral structures with a *ccp* substructure of I. Four of these are realized by HgI_2 red and orange, while $ZnCl_2$ forms a fifth simple structure not (yet) found for HgI_2, which is probably the most ionic one since it shows the most homogeneous cation distribution. The structure of red HgI_2 has also been reported for $ZnCl_2$. Interestingly, the supertetrahedral D-structure is the stable form of ZnI_2, and also a metastable form of HgI_2. CdF_2 crystallizes with the CaF_2 fluorite-type structure, as does HgF_2. The other Cd halides form the well-known octahedral layer structures of which phase IV of $HgBr_2$ is a variant. We may conclude that the group IIB difluorides follow the rules for ionic structures, CN increasing from 6 to 8 with increasing cation size. Indeed, the observed framework structures follow the classical ionic radius-ratio rule [33] surprisingly well: coordination numbers ought to be 4 for $ZnCl_2$, $ZnBr_2$, ZnI_2 ($R = r_{cation}/r_{anion} < 0.41$), 6 for ZnF_2, $CdCl_2$, $CdBr_2$, CdI_2 ($0.41 < R < 0.73$) and 8 for CdF_2, HgF_2 ($R > 0.73$). However, the other Pauling rules for ionic structures are hardly obeyed, except for the fluorides and $ZnCl_2$, since the cations do not adopt the most homogeneous distributions over the available voids of the anion packings and octahedra share too many edges. CN = 6 would also be predicted for $HgCl_2$, $HgBr_2$ and HgI_2 which in reality form molecular and tetrahedral structures (with the exception of phase IV of $HgBr_2$). Even though it is not surprising that HgI_2 in particular is far from being ionic, we regret that ab initio quantum mechanical calculations are not yet available to elucidate the preferred bonding modes of these heavy atoms.

Acknowledgements

This work has been supported by the Swiss National Science Foundation.

References

[1] M. Piechotka, Mater. Sci. Eng. 18 (1997) 1.

[2] B. Steiner, L. Van dan Berg, U. Laor, J. Appl. Phys. 86 (1999) 4677.

[3] L. Fornaro, L. Luchini, M. Köncke, L. Mussio, E. Quagliata, K. Chattopadhyay, A. Burger, J. Cryst. Growth 217 (2000) 263.

[4] M. Schieber, H. Hermon, A. Vilensky, L. Melekhov, R. Shatunovsky, E. Meerson, H. Saado, Nucl. Inst. Meth. Phys. Res. A 458 (2001) 41.

[5] R. Farrell, F. Olschner, K. Shah, M. Squillante, Nucl. Instr. Meth. Phys. Res. A 387 (1997) 194.

[6] W. Kleber, H. Raidt, K.O. Leupold, Kristall und Technik 3 (1968) 65.

[7] M. Hostettler, H. Birkedal, D. Schwarzenbach, Helv. Chim. Acta 86 (2003) 1410.

[8] J.M. Bijvoet, A. Claasen, A. Karssen, Proc. Acad. Sci. Amst. 29 (1926) 529.

[9] G.A. Jeffrey, M. Vlasse, Inorg. Chem. 6 (1967) 396.

[10] M. Hostettler, H. Birkedal, D. Schwarzenbach, Acta Crystallogr. B 58 (2002) 903.

[11] M. Hostettler, D. Schwarzenbach, Acta Crystallogr. B 58 (2002) 914.

[12] C. Guminski, J. Phase Equil. 18 (1997) 206.

[13] P.W. Bridgman, Proc. Am. Acad. Arts Sci. 72 (1937) 45.

[14] E.D. Tonkov, N.A. Tikhomirovy, Sov. Phys. Crystallogr. 15 (1971) 945.

[15] D.M. Adams, R. Appleby, J. Chem. Soc., Dalton Trans. (1977) 1535.

[16] M.Y. Khilji, W.F. Sherman, A. Stadtmuller, G.R. Wilkinson, J. Raman Spectrosc. 11 (1981) 238.

[17] H. Mikler, Monatsh. Chem. 103 (1972) 110.

[18] M. Hostettler, PhD thesis, Université de Lausanne, Switzerland, 2002.

[19] M. Hargittai, Chem. Rev. 100 (2000) 2233.

[20] J.B. Newkirk, Acta Metall. 4 (1956) 316.

[21] M. Hostettler, H. Birkedal, D. Schwarzenbach, Chimia 55 (2001) 541.

[22] P. Tolédano, V. Dmitriev, Reconstructive Phase Transitions in Crystals and Quasicrystals, World Scientific, Singapore, 1996.

[23] H. Braekken, Z. Kristallogr. 83 (1932) 222.

[24] V.I. Pakhomov, A.V. Goryunov, I.N. Ivanova-Korfini, A.A. Boguslavskii, R.S. Lotfullin, Russ. J. Inorg. Chem. 35 (1990) 1407.

[25] P.W. Bridgman, Proc. Am. Acad. Arts Sci. 72 (1937) 45.

[26] D.M. Adams, R. Appleby, J. Chem. Soc., Dalton Trans. (1977) 1535.

[27] M. Hostettler, D. Schwarzenbach, J. Helbing, V. Dmitriev, H.-P. Weber, Solid-State Commun. 129 (2004) 359.

[28] V. Subramanian, K. Seff, Acta Crystallogr. B 36 (1980) 2132.

[29] M. Hostettler, V. Dmitriev, H.-P. Weber, D. Schwarzenbach, Acta Crystallogr. A 58 (suppl.) (2002) C176.

[30] D.M. Adams, R. Appleby, J. Chem. Soc., Dalton Trans. (1977) 153.

[31] D.B. Balashov, D.A. Ikhenov, Sov. Phys. Solid State 17 (1976) 1788.

[32] F. Ebert, H. Woitinek, Z. Anorg, Allg. Chem. 210 (1933) 269.

[33] A.F. Wells, Structural Inorganic Chemistry, Clarendon Press, Oxford, UK, 1987.

[34] H.R. Oswald, H. Jaggi, Helv. Chim. Acta 43 (1960) 72.

[35] B. Brehler, Z. Kristallogr. 115 (1961) 373.

[36] P.H. Fourcroy, D. Carré, J. Rivet, Acta Crystallogr. B 34 (1978) 3160.

[37] C. Chieh, M.A. White, Z. Kristallogr. 166 (1984) 189.